# Size Control, Metal Substitution, and Catalytic Application of Cryptomelane Nanomaterials Prepared Using Cross-linking Reagents

Jia Liu,[†] Young-Chan Son,[‡] Jun Cai,[‡] Xiongfei Shen,[†] Steven L. Suib,*[,†,‡,§] and Mark Aindow[†,||]

*Institute of Materials Science, University of Connecticut, U-3136, Storrs, Connecticut 06269-3136, Department of Chemistry, University of Connecticut, U-3060, Storrs, Connecticut 06269-3060, Department of Chemical Engineering, University of Connecticut, U-3222, Storrs, Connecticut 06269-3222, and Department of Metallurgy and Materials Engineering, University of Connecticut, U-3136, Storrs, Connecticut 06269-3136*

*Received May 16, 2003. Revised Manuscript Received October 21, 2003*

A novel sol−gel-assisted solid-state synthetic method has been developed to prepare pure and transition-metal-substituted cryptomelane 1D nanomaterials with controlled particle sizes. Different cross-linking reagents (PVA, glycerol, or glucose) have been used to prepare precursor powder materials and to produce nanorods, nanoneedles, or nanowires. The phase transformation, crystal structures, and properties of these nanomaterials have been investigated using a variety of characterization techniques including XRD, TEM, SEM, FT-IR, TGA, and BET surface area measurement. Both the cross-linking reagents and nitrate were found to affect the crystalline phase transformation of the nanomaterials. The cryptomelane phase was formed around 500−600 °C in the nanomaterials depending on the type of cross-linking reagent used. The nanoscale materials exhibit long-range ordered structures along the *b* axis. No cross-linking reagent residues were found in the final products after the reactions were complete. Several types of transition metal cations ($Fe^{3+}$, $Co^{2+}$, $Ni^{2+}$, and $Cu^{2+}$) were used to substitute into cryptomelane nanomaterials. XRD data show that Fe(III) cations have been substituted into the materials without the formation of additional amorphous or crystalline phases, while the other three cations caused the formation of impure amorphous or crystalline phases. These nanomaterials showed thermal stability up to 700−800 °C. Catalytic application of these nanoscale manganese oxide materials has been explored in the green oxidation of toluene to produce benzyl alcohol, benzylaldehyde, and benzoic acid. The nanoscale catalysts showed unique catalytic activity for this oxidation compared to those catalysts conventionally used for this reaction.

## Introduction

In the past few years, one-dimensional nanoscale structures (nanowires, nanorods, and nanotubes) have been stimulating significant interest in material chemistry due to their unique electronic, magnetic, optical, and micromechanical properties.[1−8] Syntheses, properties, and applications of these nanomaterials have been of interest to many research groups. Various methods, such as laser ablation,[9] template-assisted chemical deposition,[2] and vapor deposition/transport techniques,[8] have been used to prepare one-dimensional nanoscale metals and semiconductors. The potential applications of these materials have been explored in nanoelectronic circuits, superstrong composites, functional nanostructured materials, and novel probe microscopy tips.[10,11]

Manganese oxide octahedral molecular sieve (OMS) materials have one-dimensional tunnel structures. These tunnel structures are formed by edge-shared and corner-shared $MnO_6$ octahedra.[12−20] OMS materials have mixed-

* To whom correspondence should be addressed.
[†] Institute of Materials Science.
[‡] Department of Chemistry.
[§] Department of Chemical Engineering.
[||] Department of Metallurgy and Materials Engineering.

(1) Liu, J.; Makwana, V.; Cai, J.; Suib, S. L.; Ainlow, M. *J. Phys. Chem.* **2003**, *107*, 9185−9194.
(2) (a) Martin, C. R. *Science* **1994**, *266*, 1961−1966. (b) Lakshmi, B. B.; Patrissi, C. J.; Martin, C. R. *Chem. Mater.* **1997**, *9*, 2544−2550.
(3) Lieber, C. M. *Solid State Commun.* **1998**, *107*, 607−616.
(4) Hu, J.; Ouyang, M.; Yang, P.; Lieber, C. M. *Nature* **1999**, *399*, 48−51.
(5) Peng, X.; Manna, L.; Yang, W.; Wickham, J.; Scher, E.; Kadavanich, A.; Alivisatos, A. P. *Nature* **2000**, *404*, 59−61.
(6) Kondo, Y.; Takayanagi, K. *Science* **2000**, *289*, 606−608.
(7) Cui, Y.; Lieber, C. M. *Science* **2001**, *291*, 851−853.
(8) Huang, M. H.; Mao, S.; Feich, H.; Yan, H.; Wu, Y.; Kind, H.; Weber, E.; Russo, R.; Yang, P. *Science* **2001**, *292*, 1897−1899.
(9) Morales, A. M.; Lieber, C. M. *Science* **1998**, *279*, 208−211.
(10) Lieber, C. M.; Morales, A. M.; Sheehan, P. E.; Wong, E. W.; Yang, P. One-Dimensional Nanostructures: Rational Synthesis, Novel Properties and Applications. In *Proceedings of the Robert A. Welch Foundation 40th Conference on Chemical Research: Chemistry on the Nanometer Scale*; Welch Foundation: Houston, 1997.
(11) Hu, J.; Odom, T. W.; Lieber, C. M. *Acc. Chem. Res.* **1999**, *32*, 435−445.
(12) Turner, S.; Siegel, M. D.; Buseck, P. R. *Nature* **1982**, *296*, 841−842.
(13) Burns, R. G.; Burns, V. M.; Stockman, H. W. *Am. Miner.* **1983**, *68*, 972−980.
(14) Golden, D. C.; Chen, C. C.; Dixon, J. B. *Science* **1986**, *231*, 717−719.

10.1021/cm0303989 CCC: $27.50 
Published on Web 12/23/2003

valent manganese species ($Mn^{2+}$, $Mn^{3+}$, and $Mn^{4+}$), microporous structures, large open tunnels, and high surface areas.[21−30] Cryptomelane-type manganese oxide (OMS-2) materials are a group of important OMS materials because OMS-2 materials have been widely used in catalysis, separations, chemical sensors, and batteries. Preparations, investigations, and applications of bulk OMS-2 materials have been explored extensively for the past 2 decades.[15,16,31−39] A reflux method was one route mostly used to prepare bulk OMS-2 materials.[33,34] To alter the properties of OMS-2 materials, metal cations have been doped into the tunnel or framework of OMS-2 materials via ion-exchange reactions[40] or isothermal/framework substitutions.[32−35] The doping amounts of foreign cations are limited because these cations are not easy to incorporate into the structures. The morphologies of these OMS-2 materials are either platelike or needlelike with sizes of up to several micrometers.

Nanoscale manganese oxide octahedral molecular sieve (OMS) materials with tunnel structures have been stimulating interest recently because their small particle sizes and larger surface areas can improve the performance of manganese oxide materials in applications such as catalysts and battery materials. [41−45] The methods used before for synthesizing these nanoscale OMS materials were either hydrothermal treatments to transform layered structure precursors to tunnel structure products[41−44] or redox reactions between permanganate salts and organic acids.[45] Nanoscale OMS materials had been prepared using single-type tunnel cation templates without any foreign cation doping or substitution. The quantities of products which can be prepared using the hydrothermal and redox reaction methods are limited. Faster and cheaper synthetic routes are needed for preparing nanoscale and metal-substituted OMS materials.

Here we report a novel sol−gel-assisted solid-state method to synthesize cryptomelane-type manganese oxide (OMS-2) nanorods, nanoneedles, and nanowires. In these syntheses, cross-linking reagents (PVA, glycerol, or glucose) have been used to control the sizes of the nanomaterials. This method was developed based on the use of cross-linking reagents to provide a homogeneous system for the reaction. The use of metal nitrates to utilize the oxidation properties of the nitrate anion upon heating to oxidize Mn(II) to higher oxidation states (III or IV) is also an important finding. This synthetic pathway not only shortened the time of preparation but also simplified the preparation procedure. The amount of products was limited only by the sizes of the reacting container, which makes this method very amenable to scale-up. Tunnel structures are formed spontaneously with the assistance of the tunnel cation templates. The effects of the cross-linking reagents and foreign cations on the formation and crystal structures of the final products have been studied. The chemical and physical properties of these nanoscale OMS materials also have been investigated.

Catalytic application of nanoscale OMS-2 materials has been explored in a novel green oxidation of toluene. The reaction was designed without using any acid or solvent. The nanoscale OMS-2 showed unique catalytic activity on the oxidative reaction of toluene, compared with bulk OMS-2 materials prepared using a reflux method and with conventional catalytic methods, such as liquid-phase oxidation using strong acids, vapor phase oxidation, electrochemical oxidation, and oxidative chlorination.[46] The green oxidation of toluene using nanoscale OMS-2 materials provides an environmentally friendly alternative to oxidize toluene to products such as benzyl alcohol, benzylaldehyde, and benzoic acid, which are very important raw materials in the fine chemical industry. The turnover number of the catalytic reaction using the novel OMS-2 nanomaterials was 13, which shows promising potential for industrial applications.

## Experimental Section

**1. Synthesis.** To synthesize nonsubstituted nanoscale OMS-2 materials, a sol was prepared first by dissolving 0.01 mol of potassium nitrate and 0.0046 mol of manganese nitrate salts in 50 mL of distilled water. A cross-linking reagent (PVA, glycerol, or glucose) was dissolved in 30 mL of distilled water.

(15) Golden, D. C.; Dixon, J. B.; Chen, C. C. *Clays Clay Miner.* **1986**, *34*, 511−520.
(16) Golden, D. C.; Chen, C. C.; Dixon, J. B.*Clays Clay Miner.* **1987**, *35*, 271−280.
(17) Post, J. E.; Bish, D. L. *Am. Miner.* **1988**, *73*, 861−869.
(18) Bish, D. L.; Post, J. E. *Am. Miner.* **1989**, *74*, 177−186.
(19) Post, J. E.; Veblen, D. R. *Am. Miner.* **1990**, *75*, 477−489.
(20) Post, J. E. *Proc. Natl. Acad. Sci. U.S.A.* **1999**, *96*, 3447−3454.
(21) Shen, Y. F.; Zerger, R. P.; DeGuzman, R. N.; Suib, S. L.; McCurdy, L.; Potter, D. I.; O'Young, C. L. *Science* **1993**, *260*, 511−515.
(22) Shen, Y. F.; Zerger, R. P.; DeGuzman, R. N.; Suib, S. L.; McCurdy, L.; Potter, D. I.; O'Young, C. L. *J. Chem. Soc., Chem. Commun.* **1992**, *17*, 1213−1214.
(23) Shen, Y. F.; Suib, S. L.; O'Young, C. L. *J. Am. Chem. Soc.* **1994**, *116*, 11020−11029.
(24) Suib, S. L. *Curr. Opin. Solid State Mater. Sci.* **1998**, *3*, 63−70.
(25) Brock, S. L.; Duan, N.; Tian, Z. R.; Giraldo, O.; Zhou, H.; Suib, S. L. *Chem. Mater.* **1998**, *10*, 2619−2628.
(26) Nitta, M. *Appl. Catal.* **1984**, *9*, 151−176.
(27) Wong, S. T.; Cheng, S. *Inorg. Chem.* **1992**, *31*, 1165−1172.
(28) Pereira-Ramos, J. P.; Badour, R.; Bach, S.; Baffier, N. *Solid State Ionics* **1992**, *701*, 3−56.
(29) Armstrong, A. R.; Bruce, P. G. *Nature* **1996**, *381*, 499−500.
(30) Shen, Y. F.; Suib, S. L.; O'Young, C. L. *J. Catal.* **1996**, *161*, 115−122.
(31) (a) Giovanoli, R. Balmer, B. *Chimia* **1981**, *35*, 53−55. (b) Giovanoli, R.; Faller, M. *Chimia* **1989**, *43*, 54−56.
(32) Cai, J.; Liu, J.; Willis, W. S.; Suib, S. L. *Chem. Mater.* **2001**, *13*, 2413−2422.
(33) Cai, J.; Liu, J.; Suib, S. L. *Chem. Mater.* **2002**, *14*, 2071−2077.
(34) De Guzman, R. N.; Shen, Y.-F.; Shaw, B. R.; Suib, S. L.; O'Young, C.-L. *Chem. Mater.* **1993**, *5*, 1395−1400.
(35) DeGuzman, R. N.; Shen, Y. F.; Neth, E. J.; Suib, S. L.; O'Young, C. L.; Levine, S.; Newman, J. M. *Chem. Mater.* **1994**, *6*, 815−821.
(36) Luo, J.; Zhang, Q.; Huang, A.; Suib, S. L. *Microporous Mesoporous Mater.* **2000**, *35*−*36*, 209−217.
(37) Zhang, Q.; Luo, J.; Vileno, E.; Suib, S. L. *Chem. Mater.* **1997**, *9*, 2090−2095.
(38) Ching, S.; Roark, J. L.; Duan, N.; Suib, S. L. *Chem. Mater.* **1997**, *9*, 750−754.
(39) Duan, N.; Suib, S. L.; O'Young, C. L. *J. Chem. Soc., Chem. Commun.* **1995**, *13*, 1367−1368.
(40) Feng, Q.; Kanoh, H.; Miyai, Y.; Ooi, K. *Chem. Mater.* **1995**, *7*, 148−153.
(41) Xia, G.-G.; Tong, W.; Tolentino, E. N.; Duan, N.-G.; Brock, S. L.; Wang, J.-Y.; Suib, S. L.; Ressler, T. *Chem. Mater.* **2001**, *13*, 1585−1592.
(42) Liu, J.; Cai, J.; Son, Y.; Gao, Q.; Suib, S. L.; Aindow, M. *J. Phys. Chem. B* **2002**, *106*, 9761−9768.
(43) Liu, J.; Makwana, V.; Cai, J.; Suib, S. L.; Aindow, M. Submitted for publication.
(44) (a) Wang, X.; Li, Y. *J. Am. Chem. Soc.* **2002**, *124*, 2880−2881. (b) Wang, X.; Li, Y. *Chem. Eur. J.* **2003**, *9*, 300−306.
(45) Sugantha, M.; Ramakrishnan, P. A.; Hermann, A. M.; Warmsingh, C. P.; Ginley, D. S. *Int. J. Hydrogen Energy* **2003**, *28*, 597−600.
(46) (a) McNeil, D. *Chem. Eng. Monographs* **1982**, *15*, 172−192. (b) Madhok, K. L. *Adv. Catal.* **1985**, *7*, 33−41. (c) Sheldon, R. A.; De Heij, N. *Stud. Org. Chem.* **1988**, *33*, 243−256.

The molar ratio of salts and cross-linking reagent was adjusted to be 1:2. Then the cross-linking reagent solution was added into the solution of salts. The mixture was stirred for 10−30 min at room temperature to form a homogeneous clear sol. The clear sol was then evaporated with vigorous stirring on a hot plate until the water in the solution was completely evaporated. Flame firing in the dried sols was observed, and a dry gel was formed at this point.

The dry gel was heated at 180 °C for 2 h in an electric oven, resulting in the formation of dark black powders, except for the gel containing glycerol in which the powders were formed after heating at 300 °C for 2 h. The powders were then calcined at elevated temperatures from 300 to 800 °C in 100 °C intervals for a 2-h heating at each interval, and a small part of the powders was saved at the end of each heating to study the structure transformation during heating.

To investigate the role of the cross-linking reagents and nitrate in the crystalline growing process, additional batches of sample were prepared. One batch of sample was prepared from the nitrate salts without using any cross-linking reagent. Another two batches were prepared using acetate or chloride salts as reactants instead of nitrate salts, and PVA was used as the cross-linking reagent. All the procedures followed the method described above.

For the preparation of metal-substituted OMS-2 materials, additional metal nitrate salt was added into the solution of potassium nitrate and manganese nitrate. The molar ratio of foreign cations to manganese cations was adjusted to 1:10 in all of the substitution syntheses, but the molar ratio of potassium cations to the sum of manganese cations and substituting cations were the same as those used in the preparation of nonsubstituted K−OMS-2. All of other syntheses procedures were the same as that used for nonsubstituted OMS-2 materials. The metal-substituted materials were designated as M/K−OMS-2 (M = foreign cations used in the substitution).

**2. Characterization.** Structural analysis was performed using powder X-ray diffraction (XRD) methods. XRD data were collected on a Scintag XDS 2000 diffractometer with Cu Kα radiation on the powder samples. TEM bright field (BF) images and selected area electron diffraction (SAED) data were obtained using a Philips EM420 transmission electron microscope (TEM) operating at an accelerating voltage of 100 kV. Samples for TEM analysis were prepared by placing a drop of nanoscale OMS-2 powder suspension diluted in acetone onto a holey carbon film supported by a 3-mm copper grid and allowing the solvent to evaporate.

The morphologies of the nanomaterials were studied using a Zeiss DSM 982 Gemini field emission scanning electron microscope (FESEM) with a Schottky emitter. The OMS-2 powder suspension in acetone was dispersed on AuPd-coated silicon chips that had been mounted onto the stainless steel sample holders using silver conductive paint.

Thermogravimetric analyses (TGA) were carried out on a Hi-Res TGA 2950 model thermogravimetric analyzer. The temperature ramp was 10 °C/min in $N_2$ for experimental studies on thermal stability. To study the mechanism of formation of OMS-2 materials and decomposition of cross-linking reagents, the sol−gel-assisted solid-state reaction was simulated in an air atmosphere using the thermalgravimetric analyzer. The powder samples used in the simulating experiments were those formed at 180 °C using PVA or glucose and those formed at 300 °C using glycerol. The ramping rate was programmed to simulate the elevated heating process in the furnace. The temperature was first increased from 30 to 200 °C with a ramping rate of 10 °C/min, which took about 17 min. Then the sample was heated at 200, 300, 400, 500, 600, 700, and 800 °C for 2 h at each temperature. The ramping rate between two temperature stages was 10 °C/min.

Fourier transform infrared (FTIR) spectra were collected on a Nicolet Magna-IR System 750 FT-IR spectrometer with a MCT-B detector and a KBr beam splitter. The elemental analyses on the nanoscale OMS-2 materials were carried out with a Perkin-Elmer Model 140 ICP-AES instrument. The average oxidation state (AOS) of manganese in the sample was determined using a potentiometric titration method.[32] The isothermal $N_2$ adsorption/desorption experiments on the powder samples were conducted on a Micromeritics ASAP 2010 surface area and porosimetry system. Each sample was predegassed at 200 °C for 15 h. Nitrogen gas was used as an adsorbate at liquid nitrogen temperature. Pore size distributions were measured. Surface areas were calculated by the BET method.

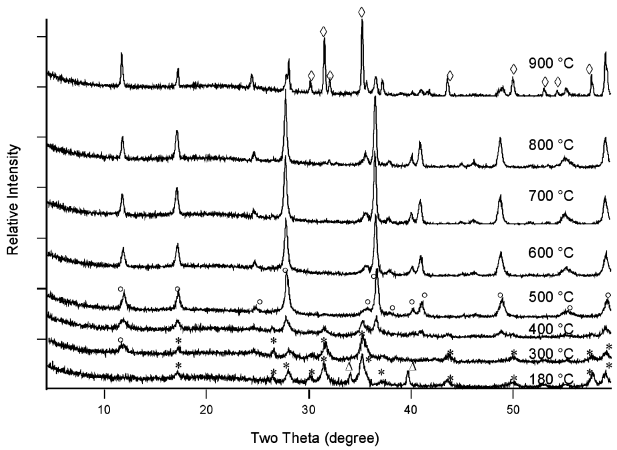


**Figure 1.** X-ray diffraction patterns of K−OMS-2 heated at different temperatures during its formation using poly(vinyl alcohol) as the cross-linking reagent. (△: potassium nitrate; *: $\gamma$-$Mn_2O_3$; ○: cryptomelane; ◇: hausmannite.)

**3. Catalytic Application.** The catalytic application was explored on the green oxidation of toluene. The activities of novel nanoscale OMS-2 materials were compared with those of bulk OMS-2 materials prepared using the reflux method.[34] The catalytic reaction was performed using a procedure which will be the subject of another paper.[47] Briefly, the catalysts were heated in an electric oven at 110 °C overnight to eliminate absorbed moisture. A solution containing 50 mmol of toluene was mixed with 0.05 g of OMS-2 and 0.03 g of 2,2′-azobisisobutyronitrile (AIBN) in a round-bottom flask. The reaction was initiated at 110 °C in UV light generated from an ultraviolet lamp for 30 min. The mixture was then stirred with refluxing at room temperature in air for 2 d. OMS-2 catalysts were removed by filtration. The filtrates were then analyzed using gas chromatography/mass spectrometry (GC/MS).

## Results

**1. XRD Studies.** X-ray diffraction was used to study the formation processes of cryptomelane by characterizing the samples saved after each heating step. A different crystalline growth process of OMS-2 was observed when a different cross-linking reagent was used.

Figure 1 shows XRD patterns of K−OMS-2 prepared using poly(vinyl alcohol) as the cross-linking reagent. At 180 °C where the dark black powders were just formed, two groups of diffraction peaks were observed in the XRD pattern, indicating the presence of crystalline phases of a small amount of potassium nitrate (JCPDS: 11-30) and a large amount of $\gamma$-$Mn_2O_3$ (JCPDS: 18-803). At 300 °C, a cryptomelane phase pattern first appeared, but the majority of the crystalline phase was still $\gamma$-$Mn_2O_3$. $\gamma$-$Mn_2O_3$ phase disappeared after heating for 2 h at 500 °C. Only the cryptomelane phase ($KMn_8O_{16}$, JCPDS: 34-168) was observed in the tem-

(47) Son, Y.-C.; Liu, J.; Ghosh, R.; Makwana, V. D.; Suib, S. L. Manuscript in preparation.

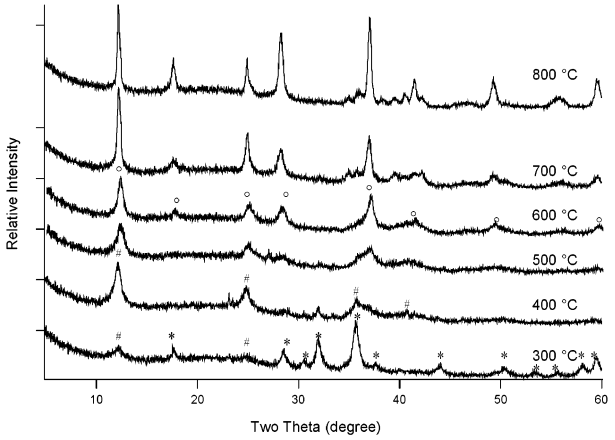


**Figure 2.** X-ray diffraction patterns of K−OMS-2 heated at different temperatures during its formation using glycerol as the cross-linking reagent. (*: $\gamma$-$Mn_2O_3$; #: birnessite; ○: cryptomelane.)

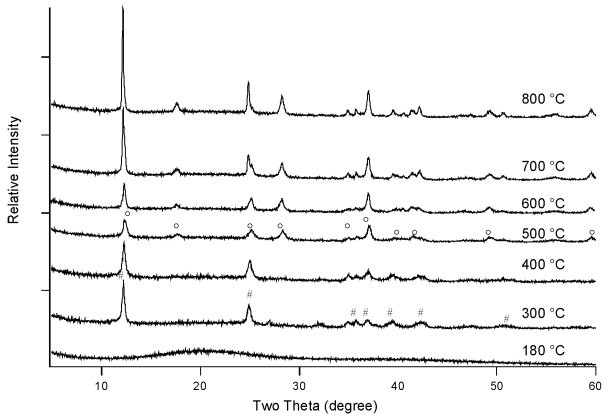


**Figure 3.** X-ray diffraction patterns of K−OMS-2 heated at different temperatures during its formation using glucose as the cross-linking reagent. (#: birnessite; ○: cryptomelane.)

perature region from 500 to 800 °C. The growth of cryptomelane crystals was indicated by the increasing intensities of the cryptomelane diffraction peaks. The growth was completed at 700 °C, as suggested by little change in the intensities of the XRD peaks of the powders heated at 700 and 800 °C. The pure crystalline phase of cryptomelane was stable up to 800 °C. At 900 °C, diffraction peaks of an impure phase appeared in the XRD pattern, which was identified as a hausmannite phase (JCPDS: 24-734).

The growing process of K−OMS-2 crystals using glycerol was different from the process when using PVA, as indicated by the XRD patterns in Figure 2. When the powder precursor was formed at 300 °C, the mixed crystalline phases of birnessite (JCPDS23-1046) and $\gamma$-$Mn_2O_3$ were observed. At 400 °C, $\gamma$-$Mn_2O_3$ phase was eliminated, leaving birnessite as the only phase in the materials. At 600 °C, the cryptomelane phase appeared. The growth of the K−OMS-2 crystal was complete at 800 °C. The hausmannite phase was also observed in the XRD pattern (not shown here) when the materials were heated at 900 °C for 2 h.

Another different formation process of cryptomelane was observed when glucose was used as the cross-linking reagent (Figure 3). At 180 °C after the black powder was just formed, no crystalline phase was formed, suggesting the powder was an amorphous

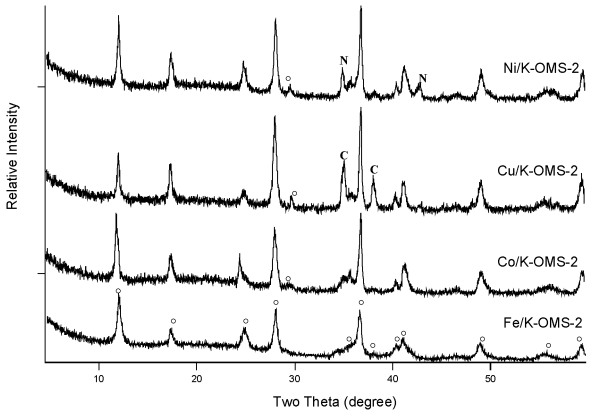


**Figure 4.** X-ray diffraction patterns of metal-substituted K−OMS-2 prepared at 800 °C using glycerol. (○: cryptomelane; C: CuO; N: NiO).

material. After the powder was heated at 300 °C for 2 h, a birnessite phase was observed in the XRD pattern. The birnessite was the only crystalline phase in the materials until 400 °C. At 500 °C, cryptomelane was formed from the birnessite, as revealed by the XRD pattern. A pure crystalline phase of cryptomelane was maintained in the temperature region from 500 to 800 °C, and the crystalline growing process was complete at 800 °C. After heating at 900 °C, a hausmannite phase was observed in the XRD pattern (not shown here).

For the sample prepared without using any cross-linking reagents, the XRD pattern (not shown here) revealed that neither $\gamma$-$Mn_2O_3$ nor birnessite phase was formed during the process. The cryptomelane phase was formed directly from the mixed salts around 600 °C with very poor crystallinity. Other impure phases were also observed in the sample at 600 °C. For the samples prepared using acetate or chloride salts, XRD data (not shown here) indicated that neither $\gamma$-$Mn_2O_3$ nor birnessite was formed as a pure phase during the heating at 300−500 °C. Impure phases were also formed along with the cryptomelane phase at 600 °C.

Figure 4 shows the XRD patterns of metal-substituted OMS-2 (Fe/K−OMS-2, Co/K−OMS-2, Ni/K−OMS-2, and Cu/K−OMS-2) prepared using glycerol at 800 °C. Cryptomelane was the only crystalline phase in the Fe- and Co-substituted materials, as revealed by the XRD data. The diffraction peak at $2\theta$ of about 30°, which was identified as the diffraction peak of (103) planes in cryptomelane, was not obviously observed in the XRD pattern of Fe/K−OMS-2 material. But this diffraction peak was observed in the other three materials. In the XRD patterns of Ni- and Cu-substituted OMS-2 materials, impure phases appeared. In the diffraction pattern of Ni/K−OMS-2, the two additional diffraction peaks at $2\theta$ of about 35° and 43° were due to diffraction from the (111) and (200) planes of nickel oxide (JCPDS4-835), respectively. In the XRD pattern of Cu/K−OMS-2, the two additional peaks at $2\theta$ of about 35.5° and 38.5° were due to diffraction from the (002) and (−111) planes of copper oxide (JCPDS41-254), respectively.

**2. HRSEM and TEM Studies.** HRSEM was used to study the morphologies of the materials. The morphologies of OMS-2 materials prepared at 800 °C with different cross-linking reagents are shown in Figure 5. The materials had a one-dimensional nanoscale structures.

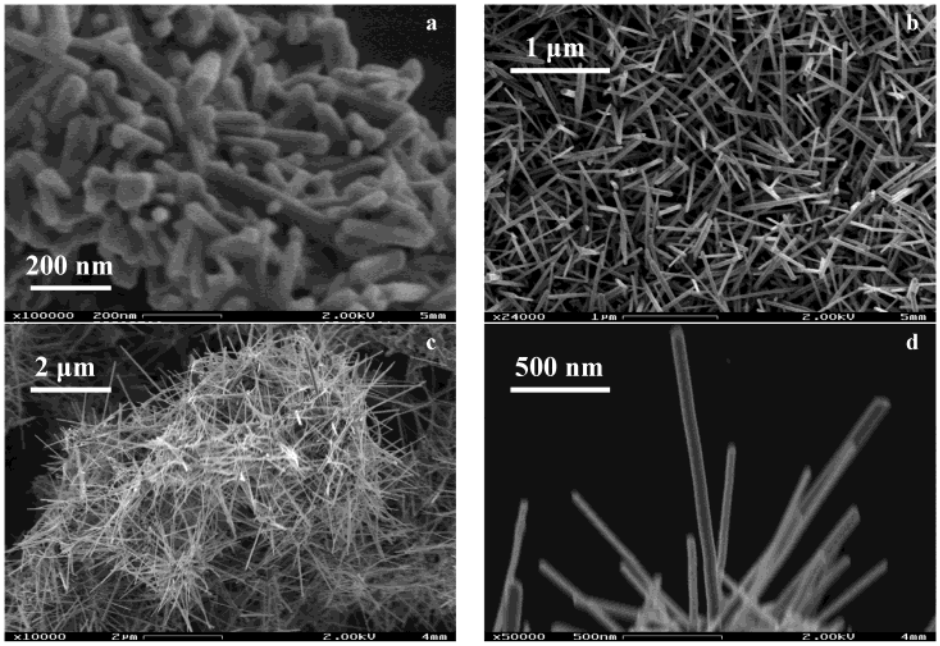


**Figure 5.** HRSEM images of K−OMS-2 nanorods prepared at 800 °C using (a) PVA and (b) glucose; (c, d) K−OMS-2 nanowires synthesized using glycerol.

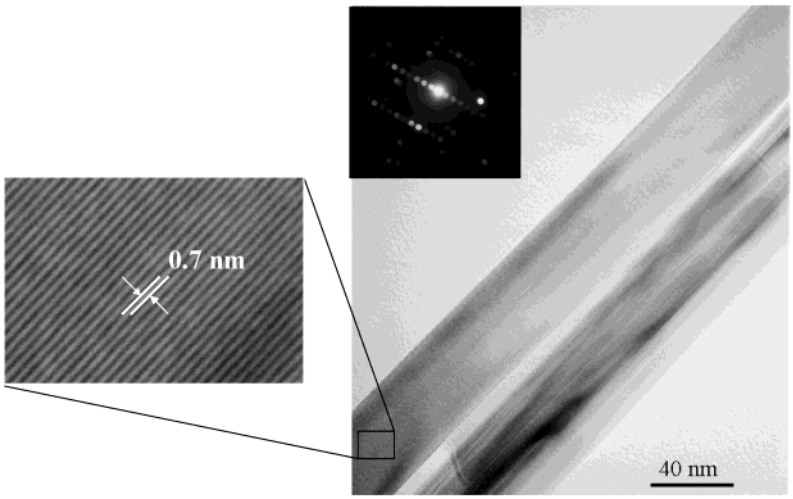


**Figure 6.** TEM bright-field image and corresponding selected area diffraction pattern of a K−OMS-2 nanowire prepared with glycerol at 800 °C.

The widths of these 1D nanocrystals ranged from 40 to 100 nm and varied depending on the cross-linking reagents. The lengths of the nanomaterials prepared using PVA were a few hundred nanometers (Figure 5a), which was the shortest among the three nanoscale K−OMS-2 materials. Intergrowth between the nanocrystals was observed in the PVA-prepared materials. The lengths of the nanocrystals prepared using glucose were a few micrometers (Figure 5b). The shapes of glucose-prepared K−OMS-2 were more uniform than those prepared with PVA. Little intergrowth was observed in the K−OMS-2 nanocrystals prepared using glucose. When glycerol was used as the cross-linking reagent, nanocrystals were formed with lengths from a few micrometers to several tens of micrometers (Figure 5c,d), which are the longest among the three nanoscale K−OMS-2. The lengths of K−OMS-2 nanocrystals prepared using different cross-linking reagents were in the following order: PVA < glucose < glycerol. To distinguish the three types of 1D nanocrystals, K−OMS-2 prepared using PVA, glucose, and glycerol were named nanorods, nanoneedles, and nanowires, respectively.

The microstructure of nanoscale OMS-2 was investigated using TEM. Figure 6 shows a TEM bright field image of a K−OMS-2 nanowire prepared at 800 °C using glycerol and the corresponding selected area electron diffraction (SAED) pattern. The tunnel structures are well-ordered continuously along the *b* axis, as indicated by the uniform lattice fringes in the enlarged image. The distance between the lattice fringes is about 0.7 nm, which corresponds to the distance between the 2 × 2 tunnels. The nanowires observed were found to lay on their (110) planes. The crystals studied using TEM showed little twinning and few dislocations in the tunnel structures, as revealed by the electron diffraction pattern and the TEM bright-field image in Figure 6. Similar microstructures and crystal orientations were observed in the nanorods prepared using PVA and in the nanoneedles prepared using glucose.

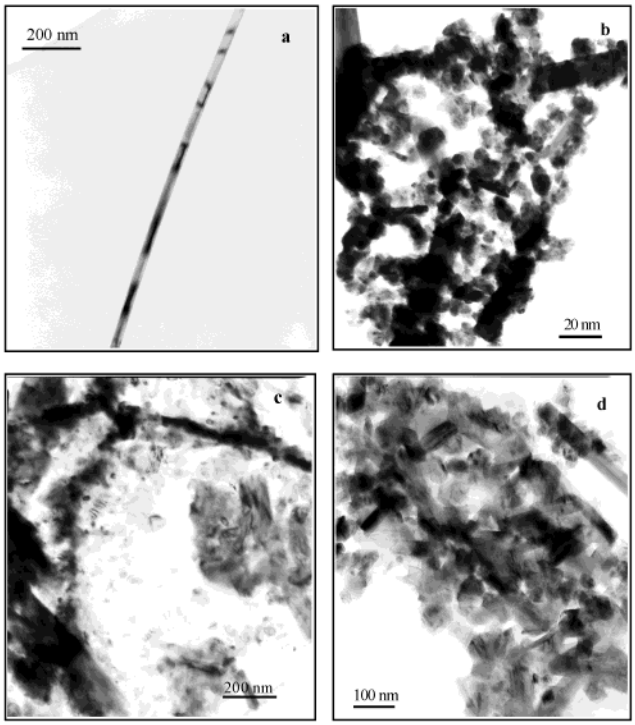


**Figure 7.** TEM bright-field images and some corresponding selected area diffraction patterns of metal-substituted nanomaterials prepared with glycerol at 800 °C: (a) Fe/K−OMS-2, (b) Co/K−OMS-2, (c) Ni/K−OMS-2, and (d) Cu/K−OMS-2.

The morphologies and microstructures of metal-substituted OMS-2 materials prepared using glycerol also were investigated using TEM. The TEM bright-field images of Fe/K−, Co/K−, Ni/K−, and Cu/K−OMS-2 are shown in Figure 7. Fe/K−OMS-2 showed similar morphologies to those of nonsubstituted K−OMS-2 nanowires prepared using glycerol (Figure 7a). The Fe/K−OMS-2 nanowires had the same electron diffraction patterns as the nonsubstituted materials (not shown here), which indicates well-formed and long-range ordered cryptomelane tunnel structures. However, other metal-substituted OMS-2 (Co/K−OMS-2, Ni/K−OMS-2, and Cu/K−OMS-2) materials showed different morphologies (Figure 7b−d). The lengths of the nanoscale OMS-2 crystals were much shorter than those of the nonsubstituted K−OMS-2 nanowires. Intergrowths between the short OMS-2 crystals were observed in these materials. Different amounts of small nanoparticles were found in these materials. Electron diffraction studies on these nanoparticles indicated that they were amorphous.

**3. FTIR Studies.** FTIR spectra of powder samples prepared with different cross-linking reagents at different temperatures are shown in Figure 8. In the spectrum of powder formed at 180 °C using PVA as the cross-linking reagent (Figure 8a), the broad band around 3450 $cm^{-1}$ and the sharp band at 1380 $cm^{-1}$ were due to the PVA and nitrate residues in the sample, respectively. At 400 °C, the intensities of these two bands decreased, indicating the amount of PVA and nitrate residues decreased in the sample. At 600 °C, the disappearance of the two bands indicated that PVA and nitrate were decomposed completely. The bands in the 450−750-$cm^{-1}$ region of the sample prepared at 800 °C were attributed to Mn−O vibrations in cryptomelane.

Figure 8b shows the FTIR spectra of the powders prepared using glycerol. Two bands at 1380 and 3460 $cm^{-1}$, which were attributed to nitrate and glycerol, were observed in the sample after heating at 600 °C. These two bands disappeared after heating at 800 °C, revealing the complete decomposition of nitrate and glycerol in the materials after heating at 800 °C.

For powders prepared using glucose at 180 °C (Figure 8c), several intense vibration bands (1060, 1660, and 3450 $cm^{-1}$) were observed in the spectra, revealing that a large amount of glucose residue was left in the materials at this temperature. The intensity of these bands decreased dramatically in the spectrum of the sample prepared at 400 °C, indicating that most of the glucose residue was decomposed in this step. The band at 1380 $cm^{-1}$ was due to nitrate residue in the sample. At 600 °C, the vibration bands of glucose and nitrate almost disappeared. These bands were not observed in the spectrum obtained for the sample prepared at 800 °C, indicating that all of the residues of nitrate and glucose were removed.

**4. TGA Studies.** Thermal stabilities of K−OMS-2 nanomaterials prepared at 800 °C using different cross-linking reagents were studied with TGA in $N_2$ in the range of 30−900 °C with a ramping rate of 10 °C/min. The TGA plots of these materials are shown in Figure 9. The thermal stabilities of the three K−OMS-2 nanomaterials varied depending on the cross-linking reagent that was used.

When PVA was used (Figure 9a), the first weight loss in the range of 30−400 °C was only 1.5%. In the range of 500−660 °C, a second weight loss (7.5%) appeared, which was due to the evolution of active oxygen species from the materials. When the temperature was higher than 800 °C, the sharp weight loss change indicated the collapse of the tunnel structure and the transformation of cryptomelane to hausmannite.

When glycerol was used (Figure 9b), the first weight loss (3%) was observed in the range of 100−150 °C, which is due to water physically absorbed in the materials. The second weight loss was about 3%, observed in the range of 600−700 °C. This weight loss was attributed to the evolution of active oxygen species in the materials. The last and sudden weight loss was observed at a temperature higher than 700 °C, where the tunnel structure collapsed.

When the glucose was used (Figure 9c), the weight loss behavior of the materials was similar to that prepared using glycerol. The first weight loss was at a temperature lower than 150 °C. The second and third weight losses were observed at 650−750 °C and at higher than 800 °C, respectively.

The TGA plots of the simulating experiments on the heating process are shown in Figure 10. For the sample using PVA as the cross-linking reagent (Figure 10a), about 6% of weight was lost in the range of 30−150 °C, which is due to physically absorbed water. During heating at 200 °C, the weight loss was only about 1%. When the temperature was ramped from 200 to 300 °C within 10 min, another 7% of weight was lost. About 1−2% more weight was lost during continuous heating at 300 °C. The weight loss was less than 0.5% when the temperature was ramped from 300 to 400 °C. During continuous heating at 400 °C, the weight loss was about

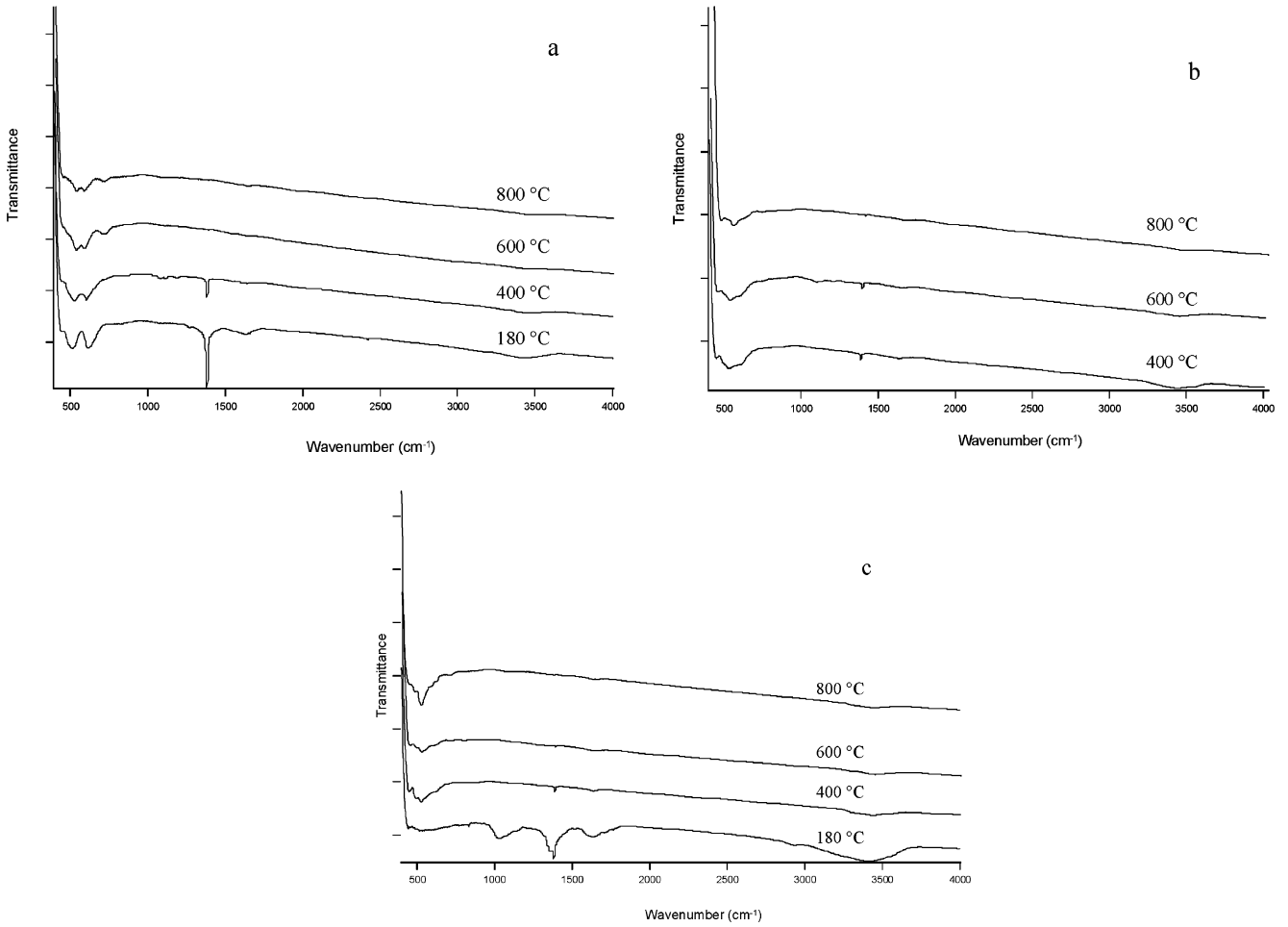


**Figure 8.** FTIR spectra of powder samples calcined at different temperature stages using (a) PVA, (b) glycerol, and (c) glucose.

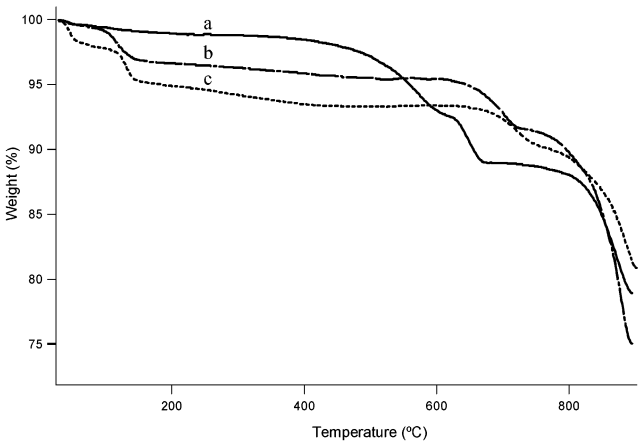


**Figure 9.** TGA plots for K−OMS-2 nanomaterials prepared at 800 °C with (a) PVA, (b) glycerol, and (c) glucose. The ramping rate is 10 °C/min in $N_2$.

1.5%. By 500 °C, the weight of the sample was not decreasing any longer. From 500 to 800 °C, the weight increased at each heating temperature. The total weight gain was about 2.5%. At 900 °C, a sudden weight loss was observed, which was due to the transformation of cryptomelane to hausmannite, as indicated by XRD data (Figure 1).

For the sample prepared using glycerol as the cross-linking reagent, a similar process of weight loss and gain was observed in the TGA plot (Figure 10b). Physically absorbed water evolved, resulting with the 7% weight loss in the range of 30−150 °C. Another two weight losses were observed around 400 and 500 °C. From 600 °C, weight gain was observed at each heating temperature until 900 °C, where the cryptomelane transformed to hausmannite. The total weight gain was about 1.2%.

The sample prepared using glucose as the cross-linking reagent had a different type of TGA plot (Figure 10c). A sudden and dramatic weight loss (∼70%) was observed around 200 °C, which indicates that most of the glucose residue was decomposed at 200 °C. In the range of 200−500 °C, an additional weight loss (∼1.5%) was observed. Then about 1.2% of weight was gained when the sample was further heated.

**5. Elemental Analysis and BET Surface Area Measurement.** The elemental composition of potassium cations, foreign cations, and manganese species in the metal-substituted OMS-2 materials was determined using the inductively coupled plasma-atomic emission spectroscopy (ICP-AES). The molar ratios of potassium to manganese and of foreign cation to manganese in Fe-, Co-, Ni-, and Cu-substituted OMS-2 materials are listed in Table 1. The molar ratios of foreign cation to manganese are much higher than those for the OMS-2 materials prepared using a conventional reflux method, which was in the range of 0.005−0.097.[48]

The $N_2$ absorption/desorption isothermal plot and the pore size distribution of K−OMS-2 nanomaterials pre-

(48) Chen, X.; Shen, Y.-F.; Suib, S. L.; O'Young, C. L. *Chem. Mater.* **2002**, *12*, 940−948.

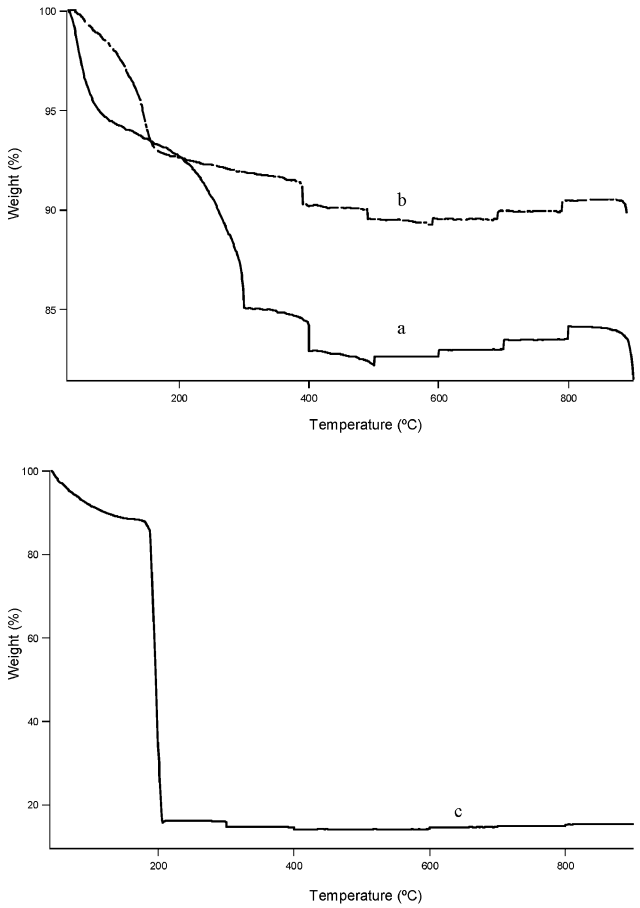


**Figure 10.** TGA plots of the simulating experiments for the solid-state reaction process in air when different cross-linking reagents were used: (a) PVA, (b) glycerol, and (c) glucose.

**Table 1. Molar Ratios of K/Mn and M/Mn (M: Foreign Cations Used in the Substitution) of Metal-Substituted OMS-2 Prepared at 800 °C Using Glycerol**

| sample name | K/Mn | M/Mn |
|---|---|---|
| Fe/K−OMS-2 | 0.26 | 0.18 |
| Co/K−OMS-2 | 0.35 | 0.17 |
| Ni/K−OMS-2 | 0.33 | 0.18 |
| Cu/K−OMS-2 | 0.33 | 0.20 |

pared at 800 °C using PVA are shown in Figure 11. The isothermal plot (Figure 11a) observed was similar to those of OMS-2 materials prepared using a conventional reflux method, indicating a Type II adsorption isotherm with micropore filling at low $p/p_0$ and capillary condensation at high $p/p_0$.[48] All of the other K−OMS-2 and metal-substituted OMS-2 had isotherms of $N_2$ absorption/desorption similar to the one in Figure 11a. The materials were microporous, as indicated by the pore size distribution plot (Figure 11b). The microporous structures of the samples prepared using the novel method in this paper are different from those prepared using a conventional reflux method. The conventional OMS-2 materials usually had only one peak in the pore size distribution plot, which was around 5 Å.[48] The nanomaterials prepared in this paper showed diverse pore size distributions with three peaks around 7.8, 9.0, and 9.8 Å. Other K−OMS-2 materials and metal-substituted OMS-2 materials also showed unusually diverse pore size distributions.

The BET surface areas of K−OMS-2 materials prepared with different cross-linking reagents and metal-substituted OMS-2 materials prepared using glycerol were measured. The results are listed in Table 2. The surface areas are lower than some OMS-2 materials that were previously reported.[43,48]

**Table 2. BET Surface Areas of K−OMS-2 Nanomaterials Prepared Using Different Cross-linking Reagents and Metal-Substituted OMS-2 Materials Prepared Using Glycerol; All of These Materials Were Calcined at 800 °C**

| sample name (cross-linking reagent used) | BET surface area ($m^2/g$) |
|---|---|
| K−OMS-2 (PVA) | 11 |
| K−OMS-2 (glycerol) | 18 |
| K−OMS-2 (sugar) | 14 |
| Fe/K−OMS-2 (glycerol) | 13 |
| Co/K−OMS-2 (glycerol) | 6 |
| Ni/K−OMS-2 (glycerol) | 6 |
| Cu/K−OMS-2 (glycerol) | 6 |

**6. Catalytic Application.** The nanoscale OMS-2 materials prepared above showed unique catalytic activity for the green oxidation of toluene. The products of the catalytic reactions included benzyl alcohol, benzylaldehyde, and benzoic acid. Both K−OMS-2 and Fe/K−OMS-2 were used as catalysts for the oxidative reaction of toluene. The conversions of the oxidative reaction using both nanoscale OMS-2 catalysts were 10−15% and the turnover numbers were about 13. The time scale for the turnover numbers was per day. When the bulk OMS-2 materials prepared using the reflux method were used, the conversion was only 3.6%. This result was based on a preliminary study using nanoscale OMS-2 for the green oxidation of organic compounds. Investigations are underway on the optimal condition for the catalytic reaction, mechanism of the oxidation of toluene, and the effects of metal substitution for the activity of the catalysts.[47]

## Discussion

**1. Effects of Cross-linking Reagents on the Formation Processes of OMS-2 Nanomaterials.** The cross-linking reagent and nitrate have influenced the formation process used for OMS-2 nanomaterials. When PVA was used as the cross-linking reagent, the solid-state reaction showed a two-step crystal growth process. The first step was around 180−500 °C where $\gamma$-$Mn_2O_3$ was formed and transformed to cryptomelane. According to the XRD patterns (Figure 1), $\gamma$-$Mn_2O_3$ first appeared as the major crystalline phase upon heating at 180 °C where the black powders were just formed. The amount of $\gamma$-$Mn_2O_3$ phase decreased at 300 °C. A cryptomelane phase appeared at 300 °C, became the major crystalline phase around 400 °C, and dominated as the only phase at 500 °C. In the same temperature range (300−500 °C), the decomposition of PVA and nitrate also occurred, as evidenced by the FTIR spectra (Figure 8a) and TGA data (Figure 10a). Nitrate was the oxidant in this step to oxidize Mn(II) species to a higher oxidation state, such as Mn(III), as evidenced by the formation of $\gamma$-$Mn_2O_3$ (see eq 1).

$$3Mn^{2+} + NO_3^- \rightarrow 3Mn^{3+} + NO_2 \qquad (1)$$

The second step of crystal growth was in the range of 500−800 °C, in which the crystals of cryptomelane kept growing and the crystallinity kept increasing, as indicated by the increasing intensities of the cryptomelane

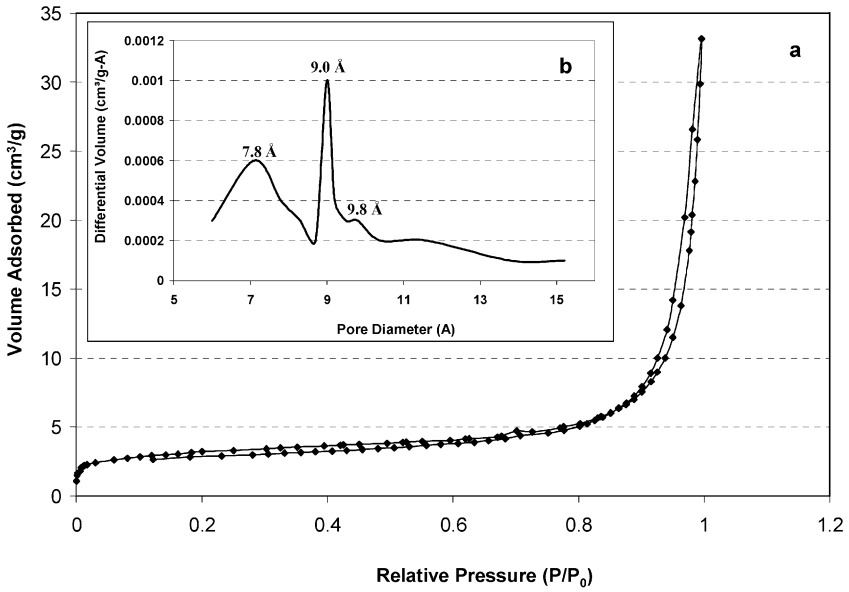


**Figure 11.** (a) $N_2$ absorption/desorption isothermal plot of K−OMS-2 nanomaterials prepared at 800 °C with PVA; (b) the corresponding pore size distribution plot of the sample.

peaks in the XRD patterns (Figure 1). Oxygen from the air took the role of oxidant in this step. This further growth of cryptomelane resulted with the increasing amount of oxygen in the structure of cryptomelane, as evidenced by the weight gain in the TGA data for this sample (Figure 10a).

When glycerol was used, the crystal growth had three steps. The first step was in the 300−400 °C range where $\gamma$-$Mn_2O_3$ was formed and transformed to birnessite, as revealed in the XRD pattern (Figure 2). At the second step of around 500−600 °C, birnessite was transformed to cryptomelane. The decomposition of glycerol and nitrate also occurred upon heating at these two steps, as revealed by their FTIR spectra (Figure 8b) and TGA data (Figure 10b). Nitrate was also the oxidant for the manganese species in these two steps. The third step was at a temperature of 600−800 °C. The crystals of cryptomelane grew upon further heating in the step where oxygen from air acted as the oxidant. Further growth of cryptomelane crystals resulted in a weight gain, which was observed in the TGA data (Figure 10b).

When glucose was used, the reaction also had a three-step phase transformation. The first step was in the temperature range of 180−400 °C, where the birnessite phase was formed in the amorphous precursor. The second step was in the range of 400−500 °C, where the birnessite phase was transformed to a cryptomelane phase. The glucose and nitrate were decomposed in these two steps, as evidenced by the TGA data (Figure 10c) and FTIR spectra (Figure 8c). The third step was in the temperature range of 500−800 °C. The manganese species were further oxidized by the oxygen in air, resulting in an increasing crystallinity of cryptomelane and the weight gain in the materials, as evidenced in the XRD patterns (Figure 3) and in the TGA experiment (Figure 10c).

Both cross-linking reagents and nitrate anions are important in the formation of well-ordered cryptomelane nanomaterials. When no cross-linking reagent was used, neither $\gamma$-$Mn_2O_3$ nor birnessite was able to be formed during heating. A small amount of cryptomelane phase was formed along with other impure phases due to the oxidative property of nitrate and oxygen from the air. This is because reactant salts were easy to aggregate without the assistance of cross-linking reagents. Therefore, reactions between the nitrate salt reactant were more rapid than those using cross-linking reagents, resulting in large particles, intergrowths, and the formation of other crystalline phases.

When nitrate was substituted with other anions (acetate or chloride), impure cryptomelane was also formed in the solid-state reaction. Nitrate acted as an oxidant in the heating and oxidation of Mn(II) to higher oxidation states at a temperature lower than 400 °C, which is evidenced by the formation of $\gamma$-$Mn_2O_3$. Without the formation of $\gamma$-$Mn_2O_3$, cryptomelane could be formed directly from the manganese and potassium salts by the oxidation of oxygen in air at temperatures as high as 600 °C, but rapid reaction between the salts caused the unavoidable formation of impure phases. The formation of $\gamma$-$Mn_2O_3$ may be critical to the formation of a pure cryptomelane phase upon further heating in air.

**2. Effects of Cross-linking Reagents and Metal Substitution on the Particle Sizes of OMS-2 Nanomaterials.** The particles sizes of the OMS-2 nanomaterials, especially the lengths along the 1D nanostructure direction, were also affected by the cross-linking reagents. The use of PVA, glucose, and glycerol resulted in nanorods, nanoneedles, and nanowires, respectively (Figure 5). This is probably related to the amount of hydroxyl groups in the cross-linking reagent, the decomposition of the cross-linking reagent during the elevated heating process, and the chemical role of the cross-linking reagents in the solid-state reaction.

When PVA or glycerol was used to prepare OMS-2 nanomaterials, $\gamma$-$Mn_2O_3$ was formed as the predominant phase at the beginning of crystal growth processes. The hydroxyl groups in the cross-linking reagent residue may have formed bonds with the surface OH groups on the manganese oxide materials, and manganese oxide particles were isolated from each other by the surround-

ing cross-linking reagents to prevent further aggregation. The ratio of hydroxyl groups to carbon atoms in glycerol is larger than that in PVA. The bond via OH groups between the manganese oxides and glycerol is stronger than that between the manganese oxides and PVA.

Since there are three hydroxyl groups in glycerol, the bonds to the manganese oxide surface are more rigid and may tend to bind to a flat surface, such as the surfaces along the length of the 1D nanostructures, rather than to a small surface, such as the tips of the nanorods. Therefore, glycerol may prevent the interaction between the surfaces along the lengths of manganese oxide nanoparticles more efficiently than PVA, but may not prevent the interaction between the tips of manganese oxide nanocrystals as well as PVA. During the reactions where glycerol was used, the nanocrystals tended to grow in a direction along the length. The diameter was not greatly changed during the calcinations, which was evidenced by HRSEM images (data are not shown here). When PVA was used, the nanocrystals tended to grow in a direction along the diameter. The diameters of PVA-prepared nanorods were almost twice the diameters of glycerol-prepared nanowires.

When glucose was used, amorphous manganese oxide was formed first. Birnessite was formed from the amorphous manganese oxides. After firing, the glucose residue may also have played a similar role as glycerol to prevent the interaction between different nanocrystals on the surfaces along their layered structure. However, interactions at the edge of the layered structures were not prevented. Nanoneedles of OMS-2 were then formed from the thin layered materials by dissociation among the layers.

The small amount of hydroxyl groups in PVA may also cause the rapid transformation from $\gamma$-$Mn_2O_3$ to cryptomelane phase without having an intermediate phase (birnessite) in the temperature range of 400−500 °C, as indicated by the XRD patterns (Figure 1). The transformations using glycerol and glucose show the intermediate birnessite phase (Figures 2 and 3) because glycerol and glucose have more hydroxyl groups, which may prevent the rapid transformation to cryptomelane.

Some of the transition-metal cations used to substitute into the OMS-2 nanomaterials have also affected the particle sizes of the final products. In the four cations used for substitution, only iron(III) cations were able to be substituted into the structure without forming other amorphous or crystalline phases, as evidenced by the XRD and TEM data. The particle shapes and sizes were similar to those of nonsubstituted OMS-2 materials prepared with the same cross-linking reagent—glycerol. When the other three cations ($Co^{2+}$, $Ni^{2+}$, and $Cu^{2+}$) were used for substitution, amorphous and crystalline impure phases were formed in the materials, as revealed by the XRD and TEM data.

The lengths of the nanoscale OMS-2 crystals were also decreased significantly. Nanosize amorphous particles were isolated from the OMS-2 materials. Fe(III) cations could be well-assembled into the structures of OMS-2 because the sizes and oxidation states of Fe(III) cation are the same as those of Mn(III) cations. The Shannon radii of $Fe^{3+}$ and $Mn^{3+}$ are both 0.645 Å.[49] Therefore, Fe(III) probably can reside in the sites of Mn(III) in the framework.[32,33] Other cations ($Co^{2+}$, $Ni^{2+}$, and $Cu^{2+}$) were not able to assemble into the OMS-2 materials due to the differences in their cation sizes from those of manganese cations. These cations may have formed metal complexes with the cross-linking reagents and prevented the binding of the cross-linking reagents with manganese oxides. Lack of glycerol binding on the surface in the long dimension of the rods resulted in the growth of the diameter of these nanomaterials.

## Conclusions

Nanorods, nanoneedles, and nanowires cryptomelane materials were successfully prepared by a novel sol−gel-assisted solid-state reaction. Cross-linking reagents played an important role in the crystal growth and controlled particle sizes of the final 1D nanostructured crystals. The nitrate anion acted as an oxidant at the early stage of the solid-state reaction to oxidize Mn(II) to Mn(III). In the second stage of oxidation, oxygen from the air was the oxidant and converted manganese species to a higher oxidation state, such as Mn(IV). Four transition-metal cations ($Fe^{3+}$, $Co^{2+}$, $Ni^{2+}$, and $Cu^{2+}$) were used to substitute into OMS-2 materials. Fe(III) cations were found to be the most suitable ones of these four cations to be associated into the structure of nanoscale OMS-2 without an impact on the crystalline structure and morphology. The other three cations showed different degrees of effects on the morphologies of the final OMS-2 materials by forming amorphous or crystalline phases. The thermal stabilities of novel synthetic OMS-2 nanomaterials were as high as 800 °C. The nanomaterials also showed an unusual pore size distribution for the micropores, compared with the OMS-2 materials that were conventionally prepared by a reflux method. Compared with conventional OMS-2 catalysts, the nanoscale OMS-2 showed exceptional catalytic activity in the green oxidation of toluene to produce benzyl alcohol, benzylaldehyde, and benzoic acid.

**Acknowledgment.** We acknowledge the funding support of the Geosciences and Biosciences Division, Office of Basic Energy Sciences, Office of Science, U.S. Department of Energy. We also thank Dr. Francis S. Galasso for useful discussion.

CM0303989

(49) Shannon, R. D. *Acta Crystallogr.* **1976**, *A32*, 751−767.